Materials & Design 265 (2026) 115936

Contents lists available at ScienceDirect

Materials & Design

journal homepage: www.elsevier.com/locate/matdes

Evaluation of the behavior of low-cost alternative TixMn alloys in Ringer's solution simulating fever and aggressive infections

Cristina Jiménez-Marcos [a], Julia Claudia Mirza-Rosca [a,b,*], Clara Mihaela Soare [c], Ionelia Voiculescu [c]

[a] Mechanical Engineering Department, Las Palmas de Gran Canaria University, Las Palmas de Gran Canaria 35001, Spain
[b] Transilvania University of Brasov, Materials Engineering and Welding Department, Brasov 500036, Romania
[c] Quality Engineering and Industrial Technology Department, Industrial Engineering and Robotics Faculty, National University of Science and Technology Politehnica Bucharest, Bucharest 060042, Romania

ARTICLE INFO

Keywords:
Titaniumalloys
Microstructuralanalysis
Microhardnesstesting
Corrosionbehavior

ABSTRACT

Among titanium (Ti) alloys, titanium-manganese alloys (TixMn, where x = 3 and 6 wt%) are highlighted for their specific strength, deformability and cold resistance, making them promising candidates for medical applications. This study investigates their microstructural characteristics, mechanical response and electrochemical behavior under various physiological conditions, including room temperature (25 °C), fever simulations (40 °C) and highly acidic environments (pH 1.2). Metallographic and scanning electron microscopy revealed equiaxed polyhedral grains with dual phase $\alpha + \beta$ microstructure. Increasing Mn content promoted β-phase stabilization confirmed by the characteristic β-phase peaks in the XRD patterns. Microhardness and nanoindentation testing showed that hardness increased with applied load and Mn content. The elastic modulus was lower than that of Ti6Al4V, suggesting improved mechanical compatibility with bone tissue. The corrosion resistance depends on environmental conditions: Ti3Mn performs best at room temperature, whereas Ti6Mn shows enhanced passivity at 40 °C due to a protective oxide layer. Both alloys are less resistant in highly acidic environments due to Mn dissolution. The studied TixMn alloys display promising structural, mechanical and electrochemical properties for biomedical applications, particularly in bone implant design, while offering a more sustainable and cost-efficient alternative to conventional Ti alloys.

1. Introduction

The development of metallic biomaterials has become pivotal in modern medicine, driven primarily by an aging population and the rising prevalence of degenerative diseases and the growing need for increasingly complex and specialized surgical interventions [1]. In this context, titanium and its alloys have established themselves as materials of choice due to their outstanding biocompatibility, high corrosion resistance and mechanical properties that allow their adequate interaction with biological tissues [2,3]. However, despite their many advantages, traditional alloys such as Ti6Al4V present certain limitations that call into question their suitability for long-term applications due to the release of aluminum (Al) ions, which is an element related to neurodegenerative illnesses and vanadium (V), which is a toxic and carcinogenic element [4–6]. Furthermore, this alloy has a much higher elastic modulus than human bone, which can lead to stress shielding [7] and hinders the proper transfer of loads to bone tissue, slowing osseointegration and accelerating bone resorption [8].

In response to these limitations, the scientific community has intensified the search for titanium alloys with new β-stabilizing elements that are biocompatible and also have a lower elastic modulus to minimize the risks associated with stress shielding [9]. In this regard, Ti-base alloys enriched with elements such as Fe [10,11], Fe-Al [12], Fe-Al- Mn [13], Fe-Mn [14], Zr [15], Mo-Zr [16], Si-Mo-Zr [17,18], Nb [19–21] or Ta [22], have been developed. Some of them have an elastic modulus that is closer to that of human bone, considerably improving the mechanical transfer between implant and tissue [4].

Although these alloys offer mechanical and chemical benefits, their elemental composition often involves limited availability and high costs. TiMn alloys have better osteoconductive properties than TiMo alloys, and clinical studies have shown that they are more favorable and economically accessible alternatives [23,24]. Mn is a non-cytotoxic

---

[*] Corresponding author at: Mechanical Engineering Department, Las Palmas de Gran Canaria University, Las Palmas de Gran Canaria, 35001, Spain
E-mail address: julia.mirza@ulpgc.es (J.C. Mirza-Rosca).

https://doi.org/10.1016/j.matdes.2026.115936
Received 7 February 2026; Received in revised form 13 March 2026; Accepted 26 March 2026

element that can improve the corrosion resistance of titanium alloys [25] and is also an essential metabolic trace element involved in antioxidant enzyme activity and physiological processes such as cellular proliferation, particularly in osteoblasts [26–29]. From the metallurgical point of view, the addition of Mn stabilizes the β-phase in titanium alloys, which allows obtaining materials with a crystalline structure that favors superior mechanical properties [30,31], such as high tensile strength, adequate ductility and an elastic modulus closer to bone tissue [3] and it can improve the corrosion resistance and antibacterial properties [32–34]. Recent studies show that TiMn alloys with concentrations between 1 and 10 wt% manganese exhibit tensile strengths between 600 and 1200 MPa and elastic moduli of approximately 85–100 GPa. These mechanical properties are comparable or even superior to those of Ti6Al4V alloys, while also showing improved osseointegration behavior [2,35–37]. Owing to the relatively low cost and high availability of Mn compared with refractory β-stabilizing elements, TiMn alloys are considered promising low-cost alternatives for biomedical titanium alloys.

In addition to mechanical properties, the biocompatibility of TiMn alloys has been improved through surface modifications, as demonstrated by both in vitro and in vivo studies. Manganese also promotes cell adhesion and osteoblast differentiation, in a way that promotes osseointegration when released into the surrounding tissues [38,39]. For example, TiO_2 coatings that are enriched with Mn tend to enhance bone cell's biological reactions by increasing integrin adhesion protein production and activating intracellular signaling pathways including the FAK (Focal Adhesion Kinase) and ERK (Extracellular signal-regulated Kinase), which are essential for stable cell adhesion and viability [40].

Metallic biomaterials used in medicine must resist corrosion in physiological environments, which can be particularly aggressive due to the presence of electrolytes, pH variations and temperature changes associated with inflammation or fever [36]. Titanium readily reacts with oxygen to form a stable oxide layer that provides high corrosion resistance in various environments. However, the effect of Mn alloying on corrosion behavior under different environmental conditions and temperatures needs further investigation to understand its effect on long-term implant stability. In this regard, preliminary research has shown that TiMn alloys maintain good corrosion resistance in simulated body fluids at 37 °C [27,37].

Currently, few studies have analyzed the corrosion behavior of biocompatible alloys under physiological specific conditions, such as simulating febrile states in patients. This study focuses on the analysis of the microstructure, mechanical behavior and electrochemical resistance of TixMn ($x = 3, 6$) alloys under simulated physiological conditions: room temperature, fever and reactive acidic environments. These variants were specifically selected to obtain a refined $\alpha + \beta$ dual-phase microstructure, seeking an optimal balance between high mechanical strength and reduced stiffness to improve compatibility with bone tissue. Furthermore, previous research by the authors has confirmed that these alloys maintain high resistance to corrosion in bodily fluids [41]. Techniques such as metallographic characterization, X-ray diffraction, microhardness testing and electrochemical testing are used to develop metallic biomaterials that achieve a balance of mechanical and chemical properties in their interaction with living tissue, thus enabling the manufacture of safer and more durable implants in different medical fields.

2. Experiment and methods

2.1. Material

The base materials used in the study were CP-Ti Grade 1 and Mn flakes of 99,9% purity. The experimental alloys were synthesized by vacuum arc remelting process in argon atmosphere (VAR) using MRF ABJ 900 equipment (Materials Research Furnaces, Allenstown, USA). To ensure compositional homogeneity, the ingots underwent six successive remelting cycles. Two TiMn alloys were obtained, named Ti3Mn (3.07 wt% Mn and Ti balance) and Ti6Mn (6.59 wt% Mn and Ti balance).

Prior to microstructural, microhardness and electrochemical characterization, the ingots were prepared through cutting and embedding in epoxy resin. Mechanical polishing was then performed using a Struers TegraPol-11 polishing system (Copenhagen, Denmark) at 150 rpm under a load of 15 N. The polishing sequence employed silicon carbide abrasive papers of progressively finer grit sizes (P400 to P2500), followed by final polishing with 0.3 µm alumina suspension on mirror-grade cloths.

2.2. Microstructural characterization

The samples were prepared for metallographic analysis in accordance with the standards set forth in ASTM E3-11(2017). The inverted microscope Olympus GX51 (Olympus GX 51, Tokyo, Japan) and SEM microscope equipped with a Z2e EDAX AMETEC (Inspect S, Eindhoven, The Netherlands) were used for the microstructure examination. At intervals of around 8–12 s, each specimen was submerged in a solution of Kroll's reagent, which is made up of 100 ml of water, 2–6 ml of nitric acid, and 1–3 ml of hydrofluoric acid. The microstructure of the samples was examined by taking micrographs of the surfaces of the samples at various magnifications.

High-resolution synchrotron X-ray diffraction measurements were conducted at the ID31 beamline of the European Synchrotron Radiation Facility (ESRF). Sample powders were loaded into cylindrical slots (approx. 1 mm thickness) and measured using transmission geometry with an incident X-ray energy of 75.051 keV ($\lambda = 0.16520$ Å). The measured intensities were collected using a Pilatus CdTe 2 M detector, with a sample-to-detector distance of approximately 1.5 m for high-resolution measurements.

2.3. Microhardness and nanoindentation testing

Microhardness testing was performed in accordance with ASTM E384-22 using a Future Tech FM-810 microhardness tester. A total of fifteen measurements were performed per specimen, each with a dwell time of 15 s. Test loads of 5, 25 and 50 gf (HV 0.005, HV 0.025 and HV 0.05, respectively) were applied. The diagonal lengths of the indentations were analyzed using iVicky software, which automatically calculated the corresponding Vickers hardness values.

The elastic modulus was determined using a Fisherscope H100 ultramicrodurometer (Helmut Fischer GmbH, Sindelfingen, Germany) following VDI/VDE 2616 Blatt 1 (2012-08). Each specimen underwent fifteen indentations. The maximum load was set to 1000 mN and applied incrementally in 25 steps, with a one-second pause between increments.

2.4. Electrochemical testing

Electrochemical behavior was evaluated in accordance with ISO 10271:2020 using a three-electrode setup: a saturated calomel electrode (SCE) as reference, a platinum counter electrode and the alloy specimen as working electrode. Sample surface areas were determined using ImageJ software. Tests were carried out in Ringeŕs solution (Grifols Laboratories, Barcelona, Spain) containing 129.90 mmol/L Na^+, 5.40 mmol/L K^+, 111.70 mmol/L Cl^-, 27.20 mmol/L lactic acid ($C_3H_6O_3$) and 1.80 mmol/L Ca^{2+}. The pH of the solution was adjusted to 1.2 using lactic acid. A BioLogic SP-150 potentiostat/galvanostat (Seyssinet-Pariset, France) was employed to perform open-circuit potential (OCP), linear polarization and electrochemical impedance spectroscopy (EIS) analyses in three different conditions: room temperature, 40 °C and pH of 1.2.

2.4.1. Corrosion potential

For OCP measurements, the "E_{corr} vs. Time" method in EC-Lab software was used over 1 h. Potentials were recorded at 30 s intervals or upon changes exceeding 100 mV, until the potential stabilizes. Results

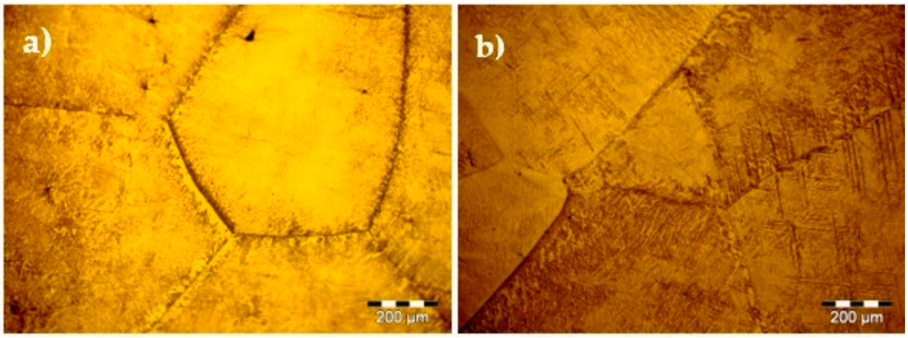

Fig. 1. Optical microstructure of as cast alloys: a) Ti3Mn; b) Ti6Mn.

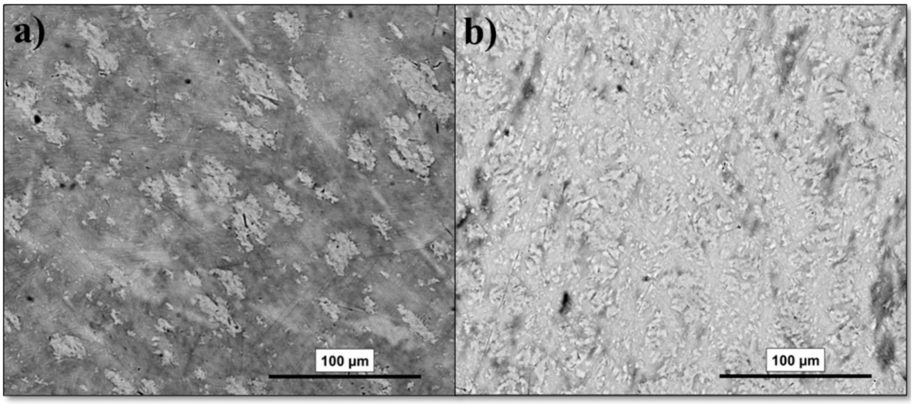

Fig. 2. SEM microstructure of as cast a) Ti3Mn and b) Ti6Mn.

were presented as potential-time curves.

2.4.2. *Corrosion rate*

Potentiodynamic polarization tests were conducted with a scan rate of 15 mV/min within a potential range of −1 to 2 V relative to SCE. Data were recorded every 0.5 s under identical environmental conditions. Corrosion rate (CR) was determined using "Tafel fit" procedure.

2.4.3. *Electrochemical impedance spectroscopy*

EIS measurements were performed by applying a potential of 0 V against the reference electrode and a frequency scan from 200 kHz to 100 mHz. Data were collected in accordance with ISO 16773–1-4:2016 and presented as Nyquist and Bode plots. Equivalent circuit (EC) modeling was applied to fit the experimental data.

3. Results and discussion

3.1. *Microstructure*

The optical microstructure of the TixMn alloys after chemical etching is shown in Fig. 1 at different magnifications. The structure consists of equiaxed polyhedral grains with clearly defined boundaries, characteristic of a titanium α + β phase mixture [37].

The slightly darker grain boundaries indicate small amounts of β-phase present along them. Since stabilization of the β-phase in titanium alloys strongly influences mechanical performance by enhancing design flexibility and broadening the range of achievable physicochemical and mechanical properties, the alloy was formulated with an increased amount of the β-stabilizer Mn (3 wt% and 6 wt%, respectively) [37]. SEM analysis (see Fig. 2a and b) confirmed the presence of a fine acicular β-titanium network and intergranular Mn-rich precipitates, which contribute to grain boundary stabilization by restricting their movement. Fig. 3 illustrates the XRD profiles obtained for the Ti3Mn and Ti6Mn alloys. The diffraction pattern clearly shows the characteristics of peaks of the β-Ti phase, corresponding to the crystallographic planes (110), (200) and (211), confirming the stabilization of this phase through the addition of manganese. Based on the current image, can be observed the reduction of the α(002) peak as we move from 3% to 6% Mn and the intensification of the β peaks, confirming the transition toward a β-rich microstructure, which is desirable for lowering the elastic modulus of biomedical Ti alloys.

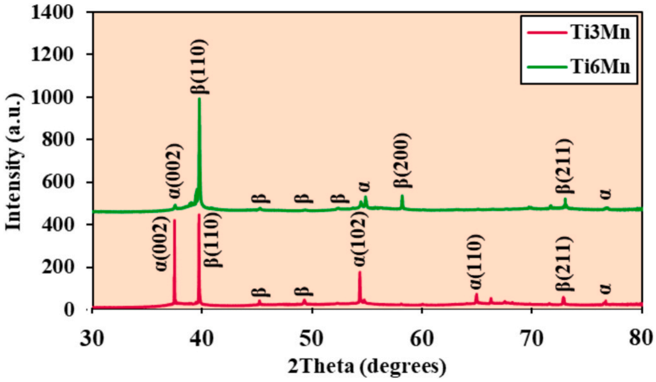

Fig. 3. X-ray diffraction (XRD) pattern of the studied alloys.

The analysis did not indicate the presence of metastable martensitic phases (α' or α''). Instead, the microstructure consists of equiaxed polyhedral grains and this is significant because the presence of martensite in as-cast titanium alloys is often associated with increased brittleness and can negatively impact on both mechanical performance and corrosion resistance.

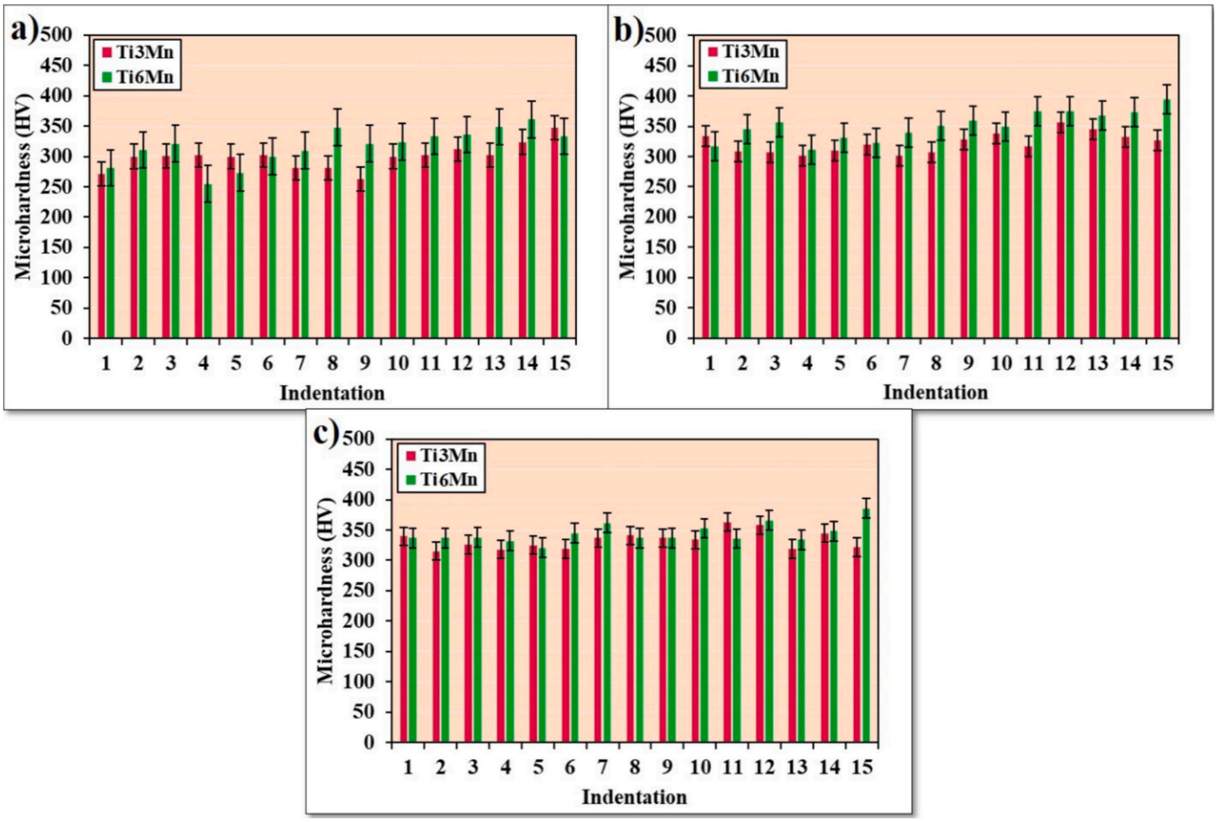

Fig. 4. Microhardness results of Ti3Mn and Ti6Mn with SD at: a) HV 0.005, b) HV 0.025 and c) HV 0.05.

Table 1
Microhardness values and footprint depth of the study samples at HV 0.005, HV 0.025 and HV 0.05.

Samples	Essay	Microhardness (HV)					Depth (μm)
		Mean	Median	SD	Maximum	Minimum	
Ti3Mn	5 gf	299	301	20	347	263	1.12
	25 gf	322	320	17	357	301	2.42
	50 gf	333	334	15	363	315	3.37
Ti6Mn	5 gf	317	321	30	361	255	1.09
	25 gf	351	351	24	394	312	2.32
	50 gf	345	337	16	386	321	3.31

The volume fractions of the α and β phases were calculated from the XRD patterns by integrating from raw XRD data the full peak area corresponding to α-Ti (002), (102), (110) and β-Ti (110), (200), (211), following methodologies reported in the literature [42–44]. The results indicate that Ti3Mn contains approximately 52 vol% α-phase and 48 vol % β-phase, while Ti6Mn contains approximately 24 vol% α-phase and 76 vol% β-phase. These results quantitatively confirm that increasing Mn content promotes β-phase stabilization in Ti-Mn alloys.

At the same time, small but distinct diffraction peaks associated with the α-Ti phase are also present. This coexistence of α and β phases is consistent with the dual-phase nature of titanium alloys and highlights the role of alloying elements in tailoring the microstructural balance and, consequently, the material´s mechanical performance.

3.2. Microhardness and nanoindentation testing

Fifteen indentations were performed on the surface of each specimen measuring HV 0.005, HV 0.025, and HV 0.05 (see Fig. 4 and Table 1). Microhardness tests were carried out across the sample surface of the sample and the results revealed that hardness values rise with increasing load while the standard deviation decreases. At lower loads, the indentation often affects only a single grain or phase, where factors such as crystallographic orientation, local Mn segregation or pores can lead to lower and more variable measurements. When the applied load is higher, the indentation covers a larger volume that encompasses multiple grains and phases, producing values that represent the bulk hardness of the alloy. As a result, the measured hardness becomes greater and shows improved consistency. It is confirmed that the indentation depth increases with the applied load, between 1.1 to 3.3 μm.

Microhardness testing was used as a localized indicator of resistance to plastic deformation and microstructural strengthening, being correlated with the strengthening mechanisms associated with alloying additions, phase distribution and grain refinement. Increased manganese content and higher applied loads resulted in higher, more consistent microhardness values, reflecting the bulk properties of the alloys rather than individual grains.

The elastic modulus obtained for Ti3Mn is 91.1 ± 0.7 GPa, lower than that of the Ti6Mn (93.9 ± 0.3 GPa) and that of Ti6Al4V alloy, which is 121.3 ± 1.2 GPa. This means that the analyzed TixMn alloys are less rigid than Ti6Al4V, thereby reducing the stress-shielding effect. The

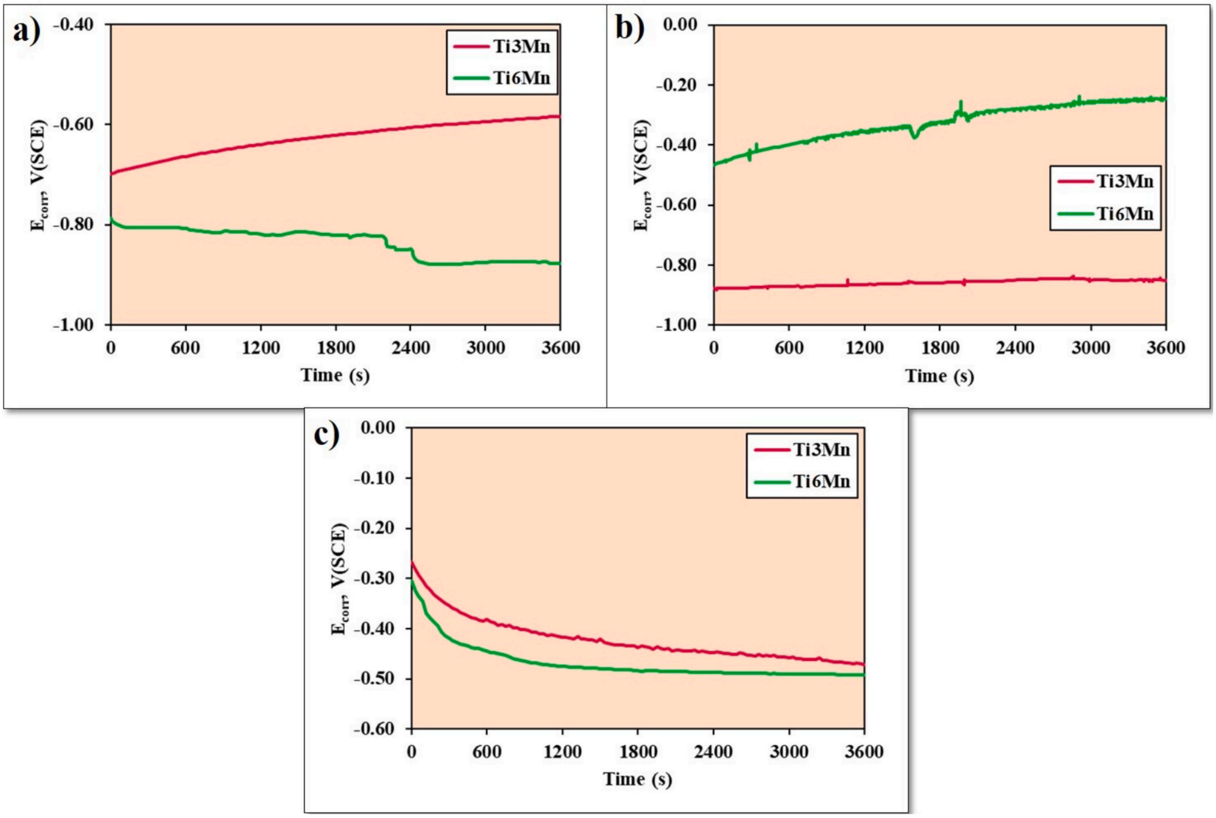

Fig. 5. A) open circuit potential curves during 1 h of immersion time of Ti3Mn and Ti6Mn in Ringer solution in different conditions: a) at room temperature, b) at 40 °C and c) with a pH 1.2.

TixMn alloy could offer an optimal compromise between mechanical strength and bone compatibility for implants compared to Ti6Al4V.

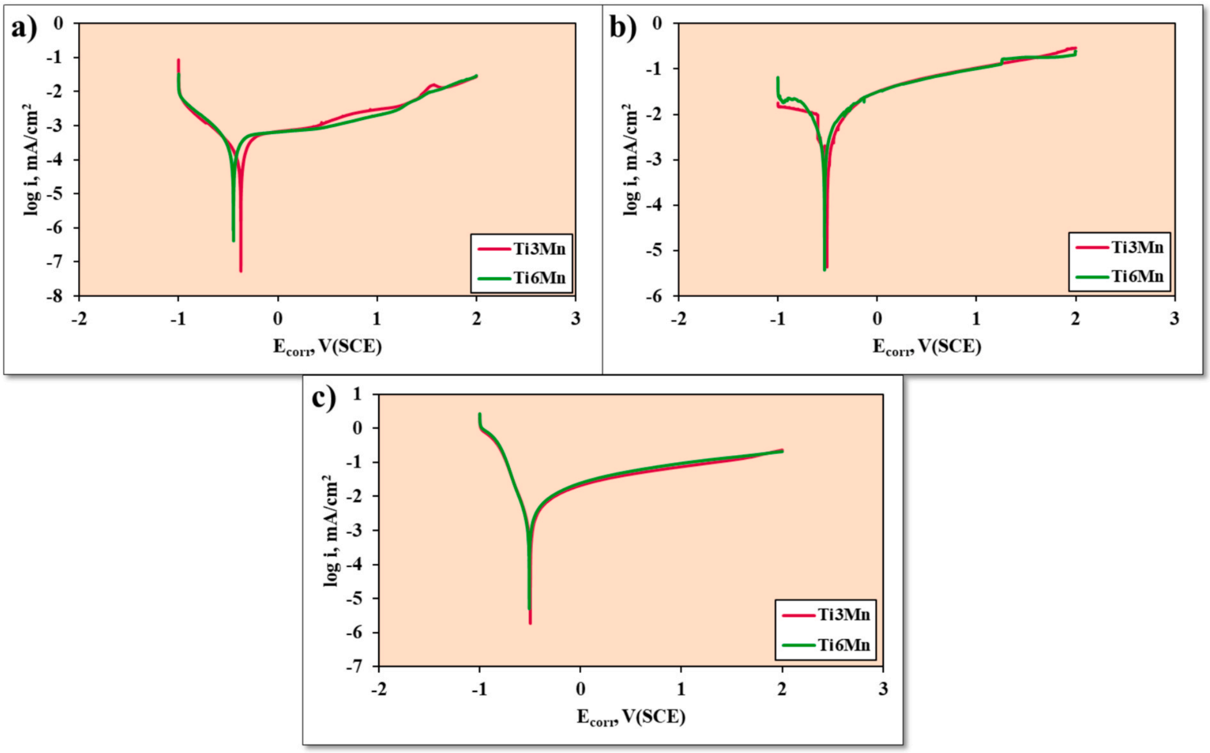

Fig. 6. Potentiodynamic curves of Ti3Mn and Ti6Mn in Ringer solution in different conditions: a) at room temperature, b) at 40 °C and c) with a pH 1.2.

Table 2
Corrosion parameters of the study samples in Ringer solution at room temperature, at 40 °C and with a pH 1.2. The lowest values under each condition are highlighted in bold for clarity.

Parameters	Ti3Mn			Ti6Mn			CP-Ti	Ti6Al4V
	Room temp.	40 °C	pH 1.2	Room temp.	40 °C	pH 1.2	Room temp.	Room temp.
E_{corr} (mV vs. SCE)	61.56	−908.00	−491.46	−563.55	−578.08	−485.32	−487.00	−545.00
i_{corr} (μA/cm^2)	$1.89 \cdot 10^{-2}$	0.89	0.35	$1.51 \cdot 10^{-2}$	0.25	0.22	$5.38 \cdot 10^{-2}$	$8.90 \cdot 10^{-2}$
β_c (mV/dec)	23.10	24.50	17.30	7.10	9.70	12.20	32.20	57.60
β_a (mV/dec)	26.90	24.80	16.50	14.10	12.30	16.20	1.52	254.00
CR (mm·year^{-1})	$8.62 \cdot 10^{-5}$	$7.79 \cdot 10^{-3}$	$7.34 \cdot 10^{-4}$	$1.32 \cdot 10^{-4}$	$2.20 \cdot 10^{-3}$	$1.93 \cdot 10^{-3}$	$4.67 \cdot 10^{-4}$	$7.64 \cdot 10^{-4}$

3.3. Electrochemical tests

A pH of 1.2 was used as a standardized model of extreme chemical stress to evaluate implant resistance by simulating the hostile acidic conditions characteristic of infected tissues. Lactic acid accumulation occurs during intense physical activity, leading to a strong burning feeling as muscles produce energy without sufficient oxygen. Mabilleau et al. [45] shown that lactic acid undermines the integrity of passive films, which minimizes the re-passivation of pure Ti implants. Moreover, it was demonstrated [46] that lactic acid negatively impacts the corrosion resistance of the alloys; at a lactic acid concentration of 0.075 wt% in Hank's solution (pH = 3), the corrosion current density grows, and the impedance of the passive film is about two-thirds of that recorded in Hank's solution at pH 7.

3.3.1. Corrosion potential

Following a 1-hour testing period in which the samples were submerged in Ringer's solution under three distinct conditions (at room temperature, at 40 °C and with the pH acidified to 1.2) the corrosion potential versus time curves of the examined samples were examined, as shown in Fig. 5. The corrosion potential, or open circuit potential (OCP), shows how likely the sample is to withstand corrosion under these conditions.

The corrosion potential of the Ti3Mn and Ti6Mn samples changed with different environments. This shows how these alloys are sensitive to environmental changes, which affects their electrochemical stability. The continuous increase in the potential of Ti3Mn at room temperature is probably may be associated with the stabilization of its passive film, while in the case of Ti6Mn, its potential drop indicates that the material was more susceptible to corrosion. Ti6Mn, however, showed continued ennoblement at 40 °C which could be related to changes in the stability

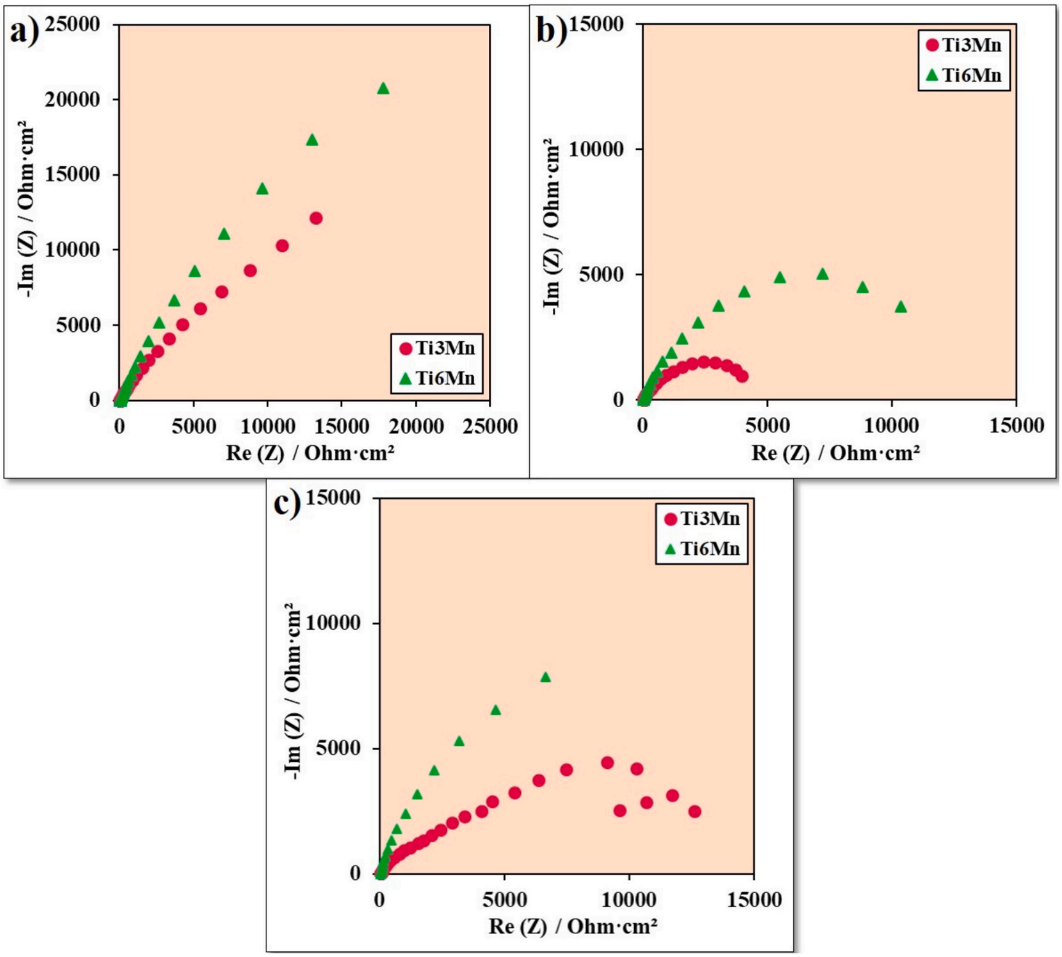

Fig. 7. Nyquist diagrams of Ti3Mn and Ti6Mn in Ringer solution in different conditions: a) at room temperature, b) at 40 °C and c) with a pH 1.2.

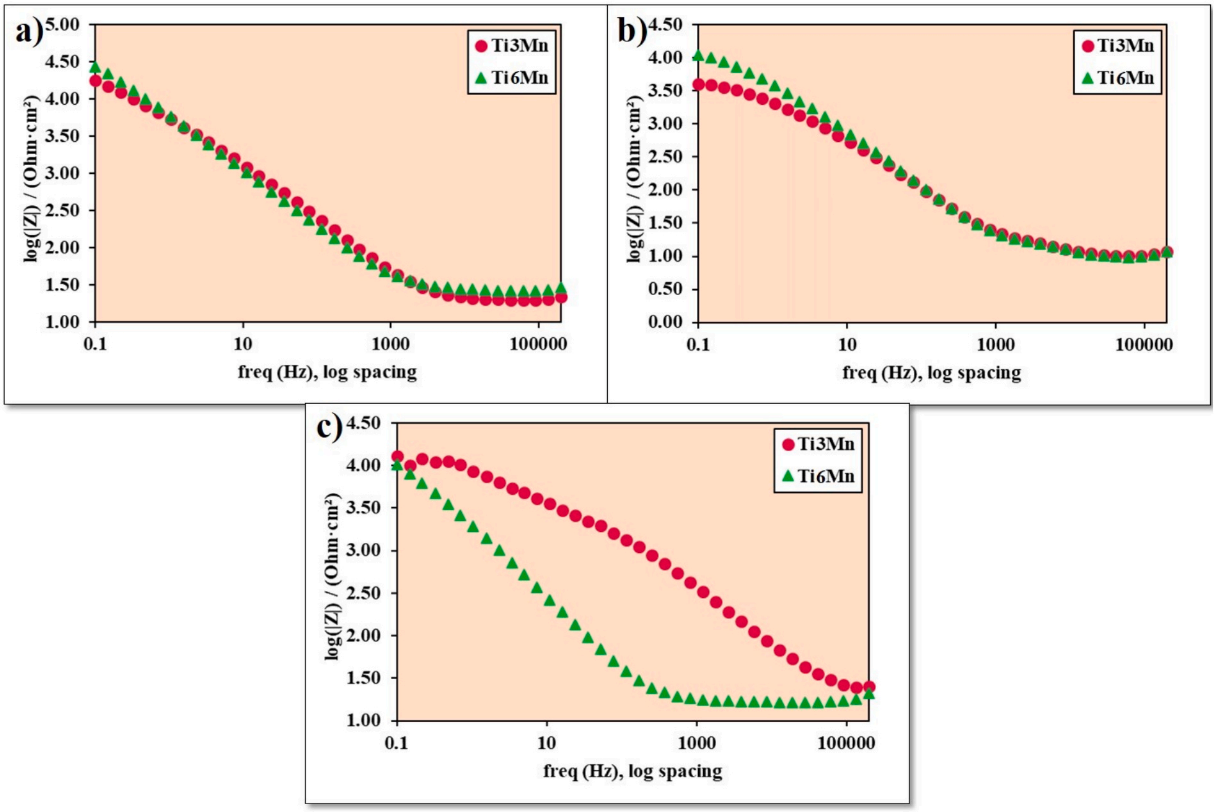

Fig. 8. Bode-|Z| diagrams of Ti3Mn and Ti6Mn in Ringer solution in different conditions: a) at room temperature, b) at 40 °C and c) with a pH 1.2.

or protective character of the surface oxide layer. Meanwhile, Ti3Mn maintained more negative potentials with limited variation, indicating a comparatively less noble behavior under these conditions. Both alloys showed a trend toward more negative potential in the acidified solution (pH 1.2) as it is in an aggressive environment. However, Ti3Mn showed slightly less negative values than Ti6Mn, suggesting higher relative corrosion resistance in acidic conditions.

3.3.2. Corrosion rate

Fig. 6 and Table 2 shows the curves and results of the potentiodynamic polarization technique used to evaluate the corrosion rate of the studied alloy in the three media. Ti3Mn in Ringer's solution at room temperature presented a combination of higher potential values and lower anodic current density values (E_{corr} and i_{corr}, respectively). In this case, lower values of I_{corr} and E_{corr} are obtained at room temperature for the Ti3Mn sample, indicating a lower corrosion rate for Ti3Mn. Subsequently, the lowest i_{corr} and E_{corr} results are those presented by Ti6Mn in Ringer's solution with a pH of 1.2.

The corrosion rate values were estimated using Tafel fitting, yielding a maximum corrosion rate value of $7.79 \cdot 10^{-3}$ mm·year^{-1} for the Ti3Mn sample at 40 °C and a minimum corrosion rate value of the same for Ti3Mn of $8.62 \cdot 10^{-5}$ mm·year^{-1} at room temperature. Nonetheless, it is noted that the corrosion rate in both samples is higher at 40 °C and lower at ambient temperature.

When compared with reference materials, both Ti3Mn and Ti6Mn exhibited lower corrosion rates than those of CP-Ti ($4.67 \cdot 10^{-4}$ mm/year) and Ti6Al4V ($7.64 \cdot 10^{-4}$ mm/year) at room temperature [47]. The enhanced corrosion resistance compared to CP-Ti may be associated with the presence of Mn, which could influence the chemistry and protective characteristics of the naturally formed passive film. In contrast to Ti6Al4V, the manganese alloys do not contain Al or V, elements with a selective dissolution and differences in their oxides stability that may lead to a less uniform and locally weaker passive film, increasing the susceptibility to electrochemical degradation. The lower corrosion rates observed for Ti3Mn and Ti6Mn could be related to differences in passive film stability, although it is necessary to confirm the exact mechanisms involved through a detailed surface characterization.

Table 3
Nyquist maxima impedance and phase angles values of Ti3Mn and Ti6Mn in Ringer solution at room temperature, at 40 °C and with a pH 1.2. The best values in each condition are highlighted in bold.

Sample	Conditions	Max impedance (Ω·cm^2)	Max phase angle (°)
Ti3Mn	Room temp.	$1.78 \cdot 10^4$	−64.12
	40 °C	$4.07 \cdot 10^3$	−64.70
	pH 1.2	$1.29 \cdot 10^4$	−58.53
Ti6Mn	Room temp.	$2.75 \cdot 10^4$	−66.35
	40 °C	$1.10 \cdot 10^4$	−72.40
	pH 1.2	$1.03 \cdot 10^4$	−75.00

3.3.3. Electrochemical impedance spectroscopy

Fig. 7 shows the Nyquist plots obtained for the two study samples when applying the corrosion potential versus SCE at the three different conditions, ranging from high to low frequencies (200 KHz to 100 mHz). Larger arcs are related to higher corrosion resistance and the deviation from a perfect semicircle indicates non-ideal capacitive behavior, possibly related to surface heterogeneity or diffusion effects. At 40 °C, the Nyquist arcs for both alloys decrease significantly compared to room temperature, indicating increased electrochemical activity due to enhanced ionic mobility and faster corrosion kinetics at elevated temperature. At pH 1.2 both alloys show distorted arcs and lower impedance values, suggesting a reduction in passive film protectiveness.

In all three conditions (Ringer's solution at room temperature, at 40 °C and pH 1.2), the Ti6Mn sample exhibits higher electrochemical

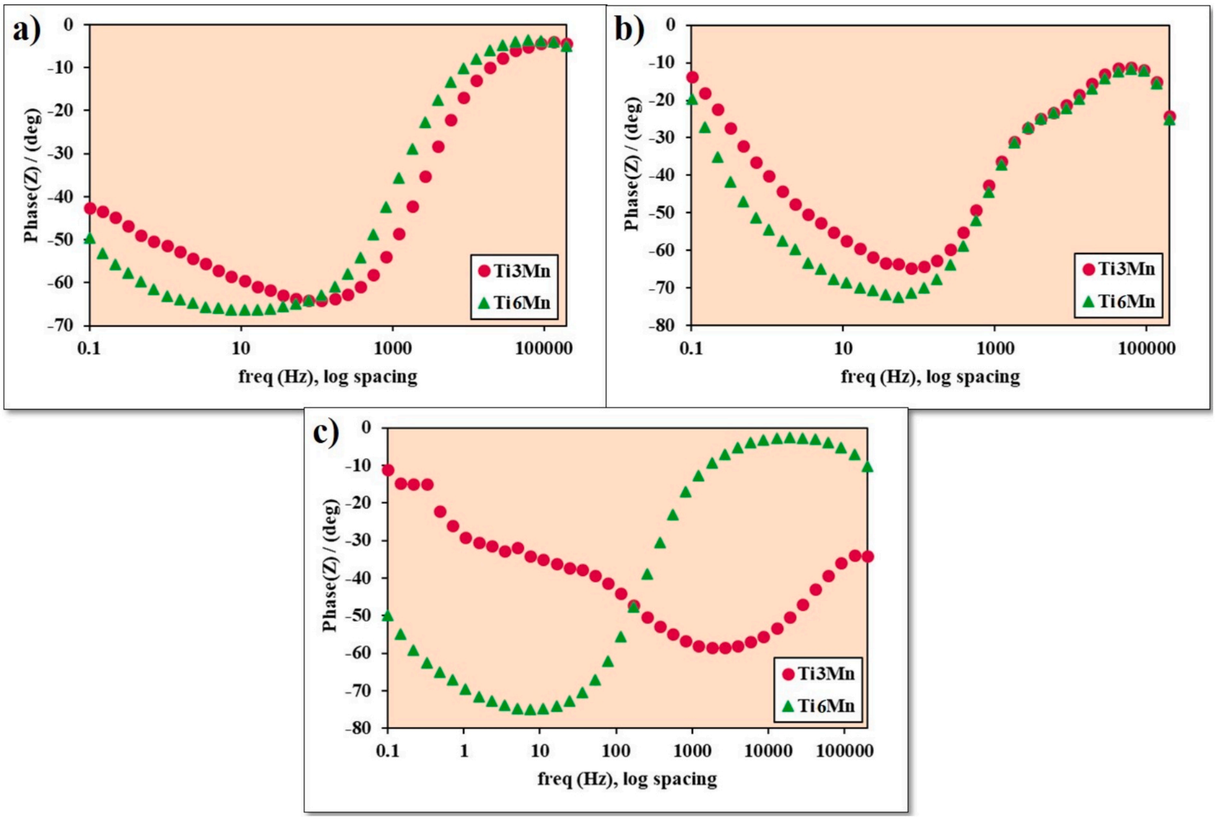

Fig. 9. Bode-phase diagrams of Ti3Mn and Ti6Mn in Ringer solution in different conditions: a) at room temperature, b) at 40 °C and c) with a pH 1.2.

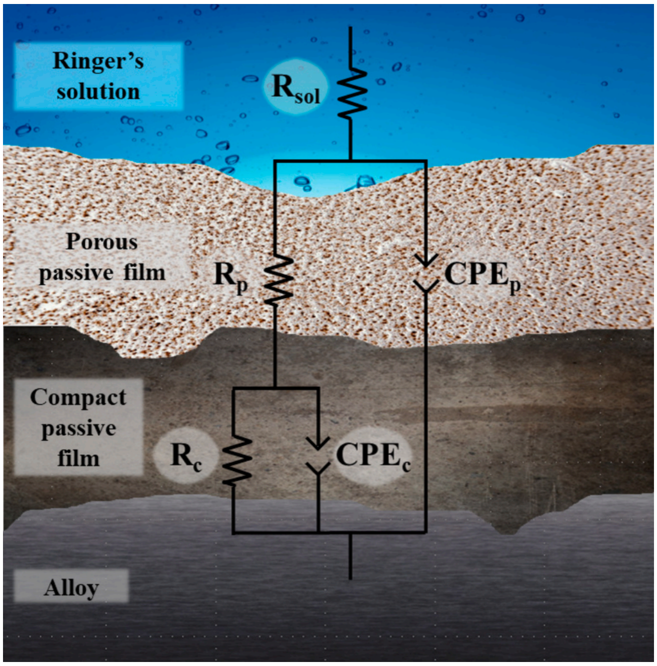

Fig. 10. Equivalent circuit $R_{sol}(CPE_p(R_p(CPE_cR_c)))$.

impedance values and corrosion resistance, indicating that the higher Mn content can promote the formation of a more stable oxide layer than the Ti3Mn sample.

The Bode impedance modulus plots of the samples immersed in Ringer's solution under all three conditions presented in Fig. 8 and Table 3 show the maximum impedance values at low frequencies. At ambient temperature and at 40 °C, both alloys exhibit effective passivation, with Ti6Mn providing slightly better protection. At pH 1.2, a more pronounced decrease in impedance is observed in Ti6Mn, indicating greater susceptibility to acid-induced dissolution. Ti3Mn retains higher IZI values across almost all the frequency range, suggesting a comparatively more stable electrochemical response under strongly acid environments.

Fig. 9 presents the Bode phase plots of the samples immersed in Ringer's solution at room temperature, 40 °C and pH 1.2 while Table 3 summarizes the maximum phase angle values. It can be observed that Ti6Mn reaches higher phase angles in most conditions, that indicates a more capacitive behavior of the surface film, consistent with the trends observed in the Bode impedance modulus plots. At 40 °C the phase angles decrease for both alloys and the phase minima shift toward higher frequencies. However, the difference between the two alloys becomes smaller, indicating that the temperature partially diminishes the beneficial effect of higher content. The acidic environment induces the most significant alterations in phase behavior.

Fig. 10 presents the analogous circuit model $R_{sol}(CPE_p(R_p(CPE_cR_c)))$, which demonstrates the greatest compatibility with the experimental findings of the research and better fit them. This model and the following equations illustrate the resistance of the Ringer solution (R_{sol}) and the presence of a double passive film, porous (R_p and CPE_p) and compact (R_c and CPE_c). The constant phase element reproduces the semi-infinite Warburg impedance (n = 0.5), resistor (n = 0.0) and capacitor (n = 1.0) as a function of the applied frequency (f) and parameter values n_p and n_c [48].

The equivalent circuit equation is shown below:

$$Z(f) = R_{sol} + \left(Y_p^0 (jw)^{n_p} + \frac{1}{R_p + \left(\left(Y_c^0 (jw)^{n_c} \right) + \frac{1}{R_c} \right)^{-1}} \right)^{-1} \tag{1}$$

Table 4
Equivalent electric circuit parameters for fitting the experimental EIS data in Ringer solution at room temperature, at 40 °C and with a pH 1.2. The higher resistance values in each condition are highlighted in bold.

Parameters	Ti3Mn			Ti6Mn		
	Room temp.	40 °C	pH 1.2	Room temp.	40 °C	pH 1.2
Q_p ($S{\cdot}sec^n/cm^2$)	$1.48{\cdot}10^{-5}$	$2.65{\cdot}10^{-8}$	$5.71{\cdot}10^{-6}$	$3.66{\cdot}10^{-5}$	$2.74{\cdot}10^{-5}$	$6.17{\cdot}10^{-5}$
n_p	0.85	1.00	0.70	0.68	0.81	0.54
R_p ($\Omega{\cdot}cm^2$)	$5.22{\cdot}10^{2}$	10.70	$3.40{\cdot}10^{3}$	2.38	$1.08{\cdot}10^{3}$	2.71
Q_c ($S{\cdot}sec^n/cm^2$)	$5.32{\cdot}10^{-5}$	$8.19{\cdot}10^{-5}$	$2.52{\cdot}10^{-5}$	$6.72{\cdot}10^{-6}$	$1.38{\cdot}10^{-4}$	$6.30{\cdot}10^{-5}$
n_c	0.48	0.74	0.71	0.91	1.00	0.93
R_c ($\Omega{\cdot}cm^2$)	$9.96{\cdot}10^{4}$	$4.43{\cdot}10^{3}$	$1.03{\cdot}10^{4}$	$9.87{\cdot}10^{4}$	$2.84{\cdot}10^{3}$	$3.85{\cdot}10^{4}$
χ^2	$7.17{\cdot}10^{-4}$	$7.41{\cdot}10^{-3}$	$6.89{\cdot}10^{-3}$	$7.99{\cdot}10^{-4}$	$2.07{\cdot}10^{-2}$	$4.68{\cdot}10^{-3}$
R_T ($\Omega{\cdot}cm^2$)	$1.00{\cdot}10^{5}$	$4.44{\cdot}10^{3}$	$1.37{\cdot}10^{4}$	$9.87{\cdot}10^{4}$	$3.92{\cdot}10^{3}$	$3.85{\cdot}10^{4}$

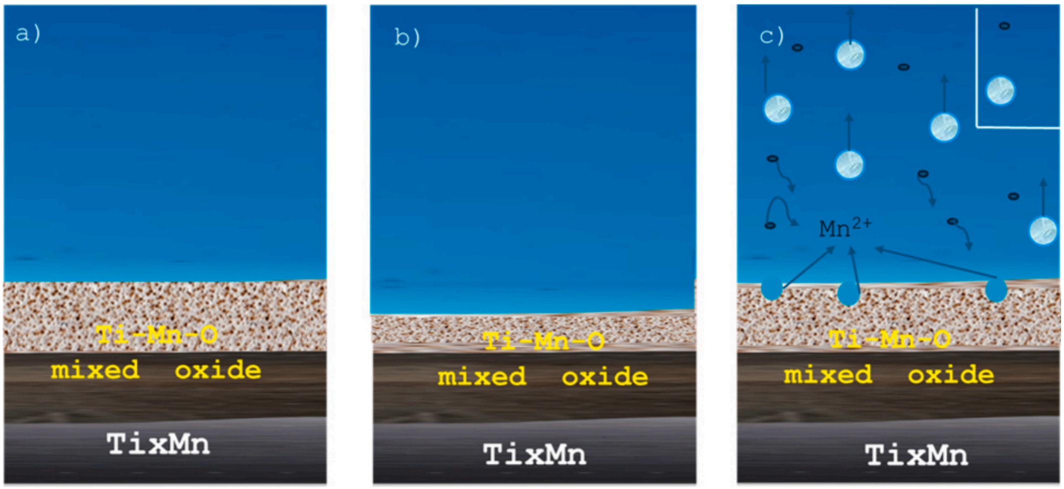

Fig. 11. Passive film at: a) room temperature; b) 40 °C and c) pH = 1.2.

The results obtained by applying the equivalent circuit R_{sol}(CPE$_p$(R_p(CPE$_c$$R_c$))) were found to agree with the experimental data. Furthermore, the chi-square values were between 10^{-3} and 10^{-4}, indicating satisfactory simulation quality. The EIS spectra obtained for all applied potentials, interpreted by the two-time equivalent circuit, can indicate the presence of a double-layer passive film on the samples' surface.

According to Table 4, the corrosion resistance values ($R_T = R_p + R_c$) of the research samples were higher in Ringer's solution at room temperature, reaching values of nearly 10^5 Ω·cm^2 while the values were lower at 40 °C, reaching approximately 10^3 Ω·cm^2, confirming the previous observations.

The main protective film on both alloys is TiO_2 which forms on the surface:

$$Ti_{(s)} + 2H_2O \rightarrow TiO_{2(s)} + 4H^+ + 4e^- \tag{2}$$

Mn is oxidized and remains as a solid oxide:

$$Mn_{(s)} + 2H_2O \rightarrow MnO_{2(s)} + 4H^+ + 4e^- \tag{3}$$

The manganese oxide may incorporate into the passive surface film, potentially modifying its electrochemical behavior [49–51]. At some conditions, especially at higher temperatures, Mn could contribute to changes in the protective characteristics of the passive layer, which may help explain the improved behavior of Ti6Mn at 40 °C (see Fig. 11).

At elevated temperatures when both oxides form and intermix, they can produce a dense mixed film:

$$xTiO_2 + yMnO_x \rightarrow Ti - Mn - Omixedoxide \tag{4}$$

At 40 °C the data suggests that Ti6Mn forms a more protective mixed oxide promoted by the elevated temperature, exhibiting enhanced passivity compared to Ti3Mn.

At low pH manganese is readily soluble as Mn^{2+} following the reaction:

$$Mn + 2H^+ \rightarrow Mn^{2+} + H_{2(g)} \tag{5}$$

If Mn dissolves, it can leave defects in the oxide film and degrade protection, explaining the poor behavior at pH = 1.2 for the Mn-richer alloy.

Under strongly acidic or highly reducing conditions, the titanium oxide can be partially converted back:

$$TiO_{2(s)} + 4H^+ + 4e^- \rightarrow Ti^{2+} or Ti^{4+} (solublespecies) + 2H_2O \tag{6}$$

The acidic environment promotes the dissolution of the oxide layer and Mn is likely to dissolve as Mn^{2+}, creating film defects; neither alloy shows a strongly protective film under these conditions and Ti6Mn is slightly worse than Ti3Mn because Mn dissolves. The dissolution of Mn and partial breakdown of TiO_2 lead to film thinning.

Different from previous work (Refs. [2,27,35–37]), which validates the mechanical viability and cytotoxicity of Ti-Mn alloys under normal physiological conditions, our study focuses on the stability of the passive layer under extreme thermal and chemical stress. We report that the behavior observed at 40 °C represents a new finding: we identify a mechanism whereby Mn promotes the formation of a denser and more protective Ti-Mn-O mixed oxide at elevated temperatures, which improves the passivity of the Ti6Mn alloy. This finding contrasts with the fragility of the material at pH 1.2, where the selective dissolution of Mn as Mn^{2+} reveals a safety limit for the use of these alloys in tissues with severe infections.

4. Conclusions

This article examines the corrosion behavior of two titanium-manganese alloys under various conditions and analyzes their microstructure, hardness and electrochemical behavior at room temperature, simulated fever and infection conditions. The main conclusions of the research are summarized below:

- Both Ti3Mn and Ti6Mn alloys exhibit a refined dual phase $\alpha + \beta$ microstructure with stabilized acicular $\alpha/\acute{\alpha}$ phases. The addition of Mn promotes β-phase stabilization, enhancing mechanical tunability and potentially improving biomedical performance.
- Ti3Mn and Ti6Mn showed increasing and more consistent hardness with higher loads while their elastic modulus values were significantly lower than those of Ti6Al4V. This indicates reduced rigidity and less stress shielding, making them promising candidates for bone implant applications.
- At room temperature, both alloys exhibited effective passivation with Ti6Mn showing slightly lower corrosion resistance rate. Increasing the temperature to 40 °C, Ti6Mn formed a more compact and protective mixed TiMn oxide layer, increasing its passivity under these conditions. Exposure to highly acidic environments led to significant degradation of the passive film in both alloys, particularly for Ti6Mn where Mn dissolution created defects and reduced film integrity.

In essence, both samples exhibited refined microstructures, favorable chemical and mechanical properties, making them promising candidates for biomedical implants where these compatibilities with bone are critical. These findings highlight the dual role of Mn in improving the passivation at elevated temperatures while compromising the corrosion resistance in strongly acidic conditions.

CRediT authorship contribution statement

Cristina Jiménez-Marcos: Writing – original draft, Software, Methodology, Investigation, Data curation, Conceptualization. **Julia Claudia Mirza-Rosca:** Writing – review & editing, Validation, Supervision, Resources, Investigation, Data curation, Conceptualization. **Clara Mihaela Soare:** Writing – original draft, Investigation, Formal analysis. **Ionelia Voiculescu:** Writing – review & editing, Visualization, Validation, Resources, Investigation, Data curation.

Declaration of competing interest

The authors declare that they have no known competing financial interests or personal relationships that could have appeared to influence the work reported in this paper.

Acknowledgements

We hereby acknowledge the European project 2023-1-RO01-KA220-HED-000159985: Smart Healthcare Engineering.

We also acknowledge the European Synchrotron Radiation Facility (ESRF) for provision of synchrotron radiation facilities and Momentum Transfer for facilitating the measurements. Jakub Drnec is thanked for assistance and support in using beamline ID31. The measurement setup was developed with funding from the European Union's Horizon 2020 research and innovation program under the STREAMLINE project (grant agreement ID 870313).

Data availability

Data will be made available on request.

References

[1] J. Quinn, R. McFadden, C.W. Chan, L. Carson, Titanium for orthopedic applications: an overview of surface modification to improve biocompatibility and prevent bacterial biofilm formation, Iscience 23 (2020) 101745, https://doi.org/10.1016/J.ISCI.2020.101745.

[2] P.F. Santos, M. Niinomi, K. Cho, M. Nakai, H. Liu, N. Ohtsu, M. Hirano, M. Ikeda, T. Narushima, Microstructures, mechanical properties and cytotoxicity of low cost beta Ti–Mn alloys for biomedical applications, Acta Biomater. 26 (2015) 366–376, https://doi.org/10.1016/j.actbio.2015.08.015.

[3] G. Senopati, R.A. Rahman Rashid, I. Kartika, S. Palanisamy, Recent development of low-cost β-Ti alloys for biomedical applications: a review, Metals (basel) 13 (2023) 194, https://doi.org/10.3390/met13020194.

[4] M. Niinomi, Mechanical properties of biomedical titanium alloys, Mater. Sci. Eng. A 243 (1998) 231–236, https://doi.org/10.1016/S0921-5093(97)00806-X.

[5] J.W. Nicholson, Titanium alloys for dental implants: a review, Prosthesis 2 (2020) 100–116, https://doi.org/10.3390/prosthesis2020011.

[6] M.L. Lourenço, F.M.L. Pontes, C.R. Grandini, The influence of thermomechanical treatments on the structure, microstructure, and mechanical properties of Ti-5Mn-Mo alloys, Metals (Basel) 12 (2022) 527, https://doi.org/10.3390/met12030527.

[7] Z. Chen, Y. Liu, H. Jiang, M. Liu, C.H. Wang, G.H. Cao, Microstructures and mechanical properties of Mn modified, Ti-Nb-based alloys, J. Alloys Compd. 723 (2017) 1091–1097, https://doi.org/10.1016/j.jallcom.2017.06.311.

[8] Y. Sun, Q. Liu, Z. Yu, L. Ren, X. Zhao, J. Wang, Study on osseointegration capability of β-Type Ti–Nb–Zr–Ta–Si alloy for orthopedic implants, Materials (basel). 17 (2024) 472, https://doi.org/10.3390/ma17020472.

[9] K. Cho, M. Niinomi, M. Nakai, H. Liu, P.F. Santos, Y. Itoh, M. Ikeda, M. abdel-hady Gepreel, T. Narushima, Improvement in mechanical strength of low-cost β-type Ti–Mn alloys fabricated by metal injection molding through cold rolling, J. Alloys Compd. 664 (2016) 272–283, https://doi.org/10.1016/j.jallcom.2015.12.200.

[10] W. Xu, X. Lu, Y. Du, Q. Meng, M. Li, X. Qu, Corrosion resistance of Ti-Fe binary alloys fabricated by powder metallurgy, Jinshu Xuebao/acta Metall. Sin. 53 (2017) 38–46, https://doi.org/10.11900/0412.1961.2016.00123.

[11] D.V. Louzguine-Luzgin, High-strength Ti-based alloys containing Fe as one of the main alloying elements, Mater. Trans. 59 (2018) 1537–1544, https://doi.org/10.2320/matertrans.M2018114.

[12] M.V. Popa, I. Demetrescu, E. Vasilescu, P. Drob, A.S. Lopez, J. Mirza-Rosca, C. Vasilescu, D. Ionita, Corrosion susceptibility of implant materials Ti-5Al-4V and Ti-6Al-4Fe in artificial extra-cellular fluids, Electrochim. Acta (2004), https://doi.org/10.1016/j.electacta.2003.12.036.

[13] J.M. Oh, C.H. Park, J.-T. Yeom, J.-K. Hong, N. Kang, S.W. Lee, High strength and ductility in low-cost Ti–Al–Fe–Mn alloy exhibiting transformation-induced plasticity, Mater. Sci. Eng. A 772 (2020) 138813, https://doi.org/10.1016/j.msea.2019.138813.

[14] W. Zheng, W. Song, T. Wu, J. Wang, Y. He, X.-G. Lu, Experimental investigation and thermodynamic modeling of the ternary Ti–Fe–Mn system for hydrogen storage applications, J. Alloys Compd. 891 (2022) 161957, https://doi.org/10.1016/j.jallcom.2021.161957.

[15] S. Grigorescu, C. Ungureanu, R. Kirchgeorg, P. Schmuki, I. Demetrescu, Various sized nanotubes on TiZr for antibacterial surfaces, Appl. Surf. Sci. 270 (2013) 190–196, https://doi.org/10.1016/j.apsusc.2012.12.165.

[16] B.-S. Sung, T.-E. Park, Y.-H. Yun, Microstructures and electrochemical behavior of Ti-Mo alloys for biomaterials, Adv. Mater. Sci. Eng. 2015 (2015) 1–7, https://doi.org/10.1155/2015/872730.

[17] C. Jimenez-Marcos, J.C. Mirza-Rosca, M.S. Baltatu, P. Vizureanu, Effect of Si contents on the properties of Ti15Mo7ZrxSi alloys, Materials (Basel) 16 (2023) 4906, https://doi.org/10.3390/MA16144906.

[18] C. Jiménez-Marcos, J.C. Mirza-Rosca, M.S. Baltatu, P. Vizureanu, Preliminary studies of new heat-treated titanium alloys for use in medical equipment, Results Eng. 25 (2025) 104477, https://doi.org/10.1016/j.rineng.2025.104477.

[19] M.-K. Han, J.-Y. Kim, M.-J. Hwang, H.-J. Song, Y.-J. Park, Effect of Nb on the microstructure, mechanical properties, corrosion behavior, and cytotoxicity of Ti-Nb alloys, Materials (Basel) 8 (2015) 5986–6003, https://doi.org/10.3390/ma8095287.

[20] V. Chakkravarthy, S.P. Jose, M. Lakshmanan, P. Manojkumar, R. Lakshmi Narayan, M. Kumaran, Additive manufacturing of novel Ti-30Nb-2Zr biomimetic scaffolds for successful limb salvage, Mater. Today Proc. 64 (2022) 1711–1716, https://doi.org/10.1016/j.matpr.2022.05.469.

[21] M.V. Popa, D. Raducanu, E. Vasilescu, P. Drob, D. Cojocaru, C. Vasilescu, S. Ivanescu, J.C.M. Rosca, Mechanical and corrosion behaviour of a Ti-Al-Nb alloy after deformation at elevated temperatures, Mater. Corros. 59 (2008), https://doi.org/10.1002/maco.200805003.

[22] I. Hulka, J.C. Mirza-Rosca, D. Buzdugan, A. Saceleanu, Microstructure and mechanical characteristics of Ti-Ta alloys before and after NaOH treatment and their behavior in simulated body fluid, Materials (Basel) 16 (2023) 1943, https://doi.org/10.3390/ma16051943.

[23] S. Swain, J.L. Ong, R. Narayanan, T.R. Rautray, Ti-9Mn β-type alloy exhibits better osteogenicity than Ti-15Mn alloy in vitro, J. Biomed. Mater. Res. Part B Appl. Biomater. 109 (2021) 2154–2161, https://doi.org/10.1002/jbm.b.34863.

[24] S.F. Jawed, C.D. Rabadia, Y.J. Liu, L.Q. Wang, P. Qin, Y.H. Li, X.H. Zhang, L. C. Zhang, Strengthening mechanism and corrosion resistance of beta-type Ti-Nb-Zr-Mn alloys, Mater. Sci. Eng. C 110 (2020) 110728, https://doi.org/10.1016/j.msec.2020.110728.

[25] T. Nishimura, Effect of microstructure on the electrochemical behavior of Ti-10 mass% Mn alloys in high chloride solution, J. Mater. Eng. Perform. 25 (2016) 443–450, https://doi.org/10.1007/s11665-015-1867-5.

[26] V. Geanta, I. Voiculescu, S. Tudoran, Effects of Fe and Mn on microstructure and microhardness of titanium alloys, Rev. Chim. 71 (2020) 87–94, https://doi.org/10.37358/RC.20.4.8046.

[27] Y. Si, Effect of manganese addition on the microstructure and mechanical properties of Ti-Nb biomedical alloys, IOP Conf. Ser.: Earth Environ. Sci 252 (2019) 022137, https://doi.org/10.1088/1755-1315/252/2/022137.

[28] M.B. Pabbruwe, O.C. Standard, C.C. Sorrell, C.R. Howlett, Bone formation within alumina tubes: effect of calcium, manganese, and chromium dopants, Biomaterials 25 (2004) 4901–4910, https://doi.org/10.1016/j.biomaterials.2004.01.005.

[29] G. Taskozhina, G. Batyrova, G. Umarova, Z. Issanguzhina, N. Kereyeva, The manganese–bone connection: investigating the role of manganese in bone health, J. Clin. Med. 13 (2024) 4679, https://doi.org/10.3390/jcm13164679.

[30] S. Ebied, A. Hamada, W. Borek, M. Gepreel, A. Chiba, High-temperature deformation behavior and microstructural characterization of high-Mn bearing titanium-based alloy, Mater Charact 139 (2018) 176–185, https://doi.org/10.1016/j.matchar.2018.03.004.

[31] M.K. Gouda, S.A. Salman, S. Ebied, Improvement in the microhardness and corrosion behaviour of Ti-14Mn biomedical alloy by cold working, Mater. Res. Express 9 (2022) 015401, https://doi.org/10.1088/2053-1591/ac4b77.

[32] Y. Xie, X. Wang, A. Xuan, Y. Li, H. Yu, E. Zhang, Effect of solid solution and aging treatment on the microstructure, mechanical properties, corrosion behavior and antimicrobial properties of Ti-5Mn alloys, Mater. Res. Express 11 (2024) 065405, https://doi.org/10.1088/2053-1591/ad5a65.

[33] A. Tanji, F. Gapsari, A. Syahrom, M.H. Idris, H. Hermawan, Effect of Mo addition on the pitting resistance of TiMn alloys in Hanks' solution, J. Alloys Compd. 871 (2021) 159582, https://doi.org/10.1016/j.jallcom.2021.159582.

[34] J.-W. Kim, M.-J. Hwang, M.-K. Han, Y.-G. Kim, H.-J. Song, Y.-J. Park, Effect of manganese on the microstructure, mechanical properties and corrosion behavior of titanium alloys, Mater. Chem. Phys. 180 (2016) 341–348, https://doi.org/10.1016/j.matchemphys.2016.06.016.

[35] P.F. Santos, M. Niinomi, H. Liu, K. Cho, M. Nakai, Y. Itoh, T. Narushima, M. Ikeda, Fabrication of low-cost beta-type Ti–Mn alloys for biomedical applications by metal injection molding process and their mechanical properties, J. Mech. Behav. Biomed. Mater. 59 (2016) 497–507, https://doi.org/10.1016/j.jmbbm.2016.02.035.

[36] Y. Alshammari, F. Yang, L. Bolzoni, Mechanical properties and microstructure of Ti-Mn alloys produced via powder metallurgy for biomedical applications, J. Mech. Behav. Biomed. Mater. 91 (2019) 391–397, https://doi.org/10.1016/j.jmbbm.2018.12.005.

[37] Y. Alshammari, S. Mendoza, F. Yang, L. Bolzoni, Effect of Mn on the Properties of Powder Metallurgy Ti-2.5Al-xMn Alloys, Materials (Basel) 16 (2023) 4917, https://doi.org/10.3390/ma16144917.

[38] Y.T. Li, D.L. Ma, H.Y. Liu, P.P. Jing, Y.L. Gong, Z. Ayaz, F.J. Jing, X. Jiang, Y. X. Leng, Biocompatibility of Ti-Mn-N films with different manganese contents, Surf. Coatings Technol. 403 (2020) 126354, https://doi.org/10.1016/j.surfcoat.2020.126354.

[39] S.-Y. Park, H.-C. Choe, Mn-coatings on the micro-pore formed Ti-29Nb-xHf alloys by RF-magnetron sputtering for dental applications, Appl. Surf. Sci. 432 (2018) 278–284, https://doi.org/10.1016/j.apsusc.2017.08.023.

[40] Z. Zhang, B. Gu, W. Zhang, G. Kan, J. Sun, The enhanced characteristics of osteoblast adhesion to porous Zinc–TiO2 coating prepared by plasma electrolytic oxidation, Appl. Surf. Sci. 258 (2012) 6504–6511, https://doi.org/10.1016/j.apsusc.2012.03.067.

[41] C.M. Soare, C. Jimenez-Marcos, S. Brito-Garcia, J.C. Mirza-Rosca, I. Voiculescu, Corrosion behavior of biocompatible Ti3Mn alloy in different physiological conditions for biomedical applications, Materials (Basel) 18 (2025) 4346, https://doi.org/10.3390/ma18184346.

[42] Y.-F. Zhang, L.-Y. Chen, Y. Liu, H.-Y. Yang, J.-H. Peng, C. Zheng, L. Zhang, L.-C. Zhang, Corrosion behavior of NiTi alloys fabricated by laser powder bed fusion in relation to the formed passive films in Hank's solution, J. Mater. Res. Technol. 34 (2025) 1933–1946, https://doi.org/10.1016/j.jmrt.2024.12.182.

[43] H. Liu, Z.-X. Wang, J. Cheng, N. Li, S.-X. Liang, L. Zhang, F. Shang, D. Oleksandr, L.-Y. Chen, Nb-content-dependent passivation behavior of Ti–Nb alloys for biomedical applications, J. Mater. Res. Technol. 27 (2023) 7882–7894, https://doi.org/10.1016/j.jmrt.2023.11.203.

[44] C. Xu, L.Y. Chen, C.B. Zheng, H.Y. Zhang, C.H. Zhao, Z.X. Wang, S. Lu, J.W. Zhang, L.C. Zhang, Improved wear and corrosion resistance of microarc oxidation coatings on Ti–6Al–4V alloy with ultrasonic assistance for potential biomedical applications, Adv. Eng. Mater. 23 (2021) 1–14, https://doi.org/10.1002/adem.202001433.

[45] G. Mabilleau, S. Bourdon, M.L. Joly-Guillou, R. Filmon, M.F. Baslé, D. Chappard, Influence of fluoride, hydrogen peroxide and lactic acid on the corrosion resistance of commercially pure titanium, Acta Biomater. 2 (2006) 121–129, https://doi.org/10.1016/j.actbio.2005.09.004.

[46] X. Wen, S. Hao, S. Liu, J. Cheng, Y. He, L.-Y. Chen, Microstructure and corrosion behavior of Ti–10Mo–6Zr–4Sn–3 Nb (Ti-B12) alloys as biomedical material in lactic acid-containing Hank's solution, Int. J. Electrochem. Sci. 20 (2025) 100974, https://doi.org/10.1016/j.ijoes.2025.100974.

[47] H. Kovacı, K. Şenel, M.T. Acar, Y.B. Bozkurt, A. Çelik, Comparative investigation of structural, morphological, mechanical, tribological and electrochemical properties of TiO2 films formed on Cp-Ti, Ti6Al4V and Ti45Nb alloys, Surf. Coatings Technol. 487 (2024) 131024, https://doi.org/10.1016/j.surfcoat.2024.131024.

[48] F. Almeraya-Calderón, J.M. Jáquez-Muñoz, M. Lara-Banda, P. Zambrano-Robledo, J.A. Cabral-Miramontes, A. Lira-Martínez, F. Estupinán-López, C. Gaona Tiburcio, Corrosion behavior of titanium and titanium alloys in Ringeŕs solution, Int. J. Electrochem. Sci. 17 (2022) 220751, https://doi.org/10.20964/2022.07.55.

[49] Y.-W. Cui, L.-Y. Chen, P. Qin, R. Li, Q. Zang, J. Peng, L. Zhang, S. Lu, L. Wang, L.-C. Zhang, Metastable pitting corrosion behavior of laser powder bed fusion produced Ti-6Al-4V in Hank's solution, Corros. Sci. 203 (2022) 110333, https://doi.org/10.1016/j.corsci.2022.110333.

[50] Y.-W. Cui, L.-Y. Chen, Y.-H. Chu, L. Zhang, R. Li, S. Lu, L. Wang, L.-C. Zhang, Metastable pitting corrosion behavior and characteristics of passive film of laser powder bed fusion produced Ti–6Al–4V in NaCl solutions with different concentrations, Corros. Sci. 215 (2023) 111017, https://doi.org/10.1016/j.corsci.2023.111017.

[51] S. Hao, X.-M. Wen, J. Cheng, X.-Y. Yao, W.-Y. Huang, R.-F. Li, L.-Y. Chen, Tailoring corrosion resistance of laser powder bed fusion produced Ti-6Al-4V via heat treatment at 700 °C in potential biomedical applications: microstructural evolution and electrochemical behavior, Met. Adv. 39 (2026) 83–94, https://doi.org/10.1016/j.metadv.2026.01.001.